Key Coverage Matters: Semi-Structured Extraction of OCR Clinical Reports

Yu Wang *AI Starfish*
Hangzhou, China

Yingyun Li *AI Starfish*
Hangzhou, China

Ying Qin *AI Starfish*
Hangzhou, China

Haiyang Qian HAIYANG.QIAN@AISTARFISH.COM *AI Starfish*
Hangzhou, China

Abstract

This work addresses a cross-institution workflow in which patients present paper or scanned reports from prior visits because relevant records are not available in the receiving hospital's EHR. This hinders not only electronic health record (EHR) integration and longitudinal review, but also downstream workflows that depend on more complete patient records, including cross-institution EHR back-fill, longitudinal follow-up for chronic disease and oncology, and report-derived clinical-trial eligibility screening. Although optical character recognition (OCR) can digitize such reports, reliable extraction remains challenging because clinical documents are heterogeneous, OCR text is noisy, and many healthcare settings require low-cost on-premise deployment.

We formulate this problem as canonical key-conditioned extractive question answering and maintain a canonical inventory and alias mapping through iterative key mining, normalization, clustering, and incremental human verification. On the 849-report development set, inventory expansion increases end-to-end Exact recall from 0.3534 to 0.8042, with Exact F1 peaking at 0.8232 for Top-95. A supplementary gold-key-conditioned comparison shows that a compact 0.2B BERT–BiLSTM–CRF extractor runs substantially faster than LoRA-adapted Qwen3 models on the same GPU, with a modest trade-off in Exact F1. An independent downstream study found task-dependent effects of structured fields, including gains of 3.27 percentage points for histologic grade and 3.52 points for treatment response, but the effects were not uniformly positive across tasks; this study evaluates representation utility rather than the proposed extractor. Although the corpus is Chinese, the method is based on the language-agnostic key–value organization of semi-structured clinical reports and can be adapted to other settings with an appropriate canonical inventory and alias mapping.

Keywords: OCR-derived clinical reports, semi-structured information extraction, key-conditioned extraction, canonical key coverage, healthcare interoperability, on-premise deployment, longitudinal patient records, clinical document processing

1. Introduction

Privacy constraints and institutional data silos can leave prior records outside the receiving hospital's EHR. The workflow considered in this study arises when patients present paper or scanned reports from previous visits to convey relevant medical history. Figure 1 depicts this scenario. This practice poses significant challenges for both clinicians and patients.

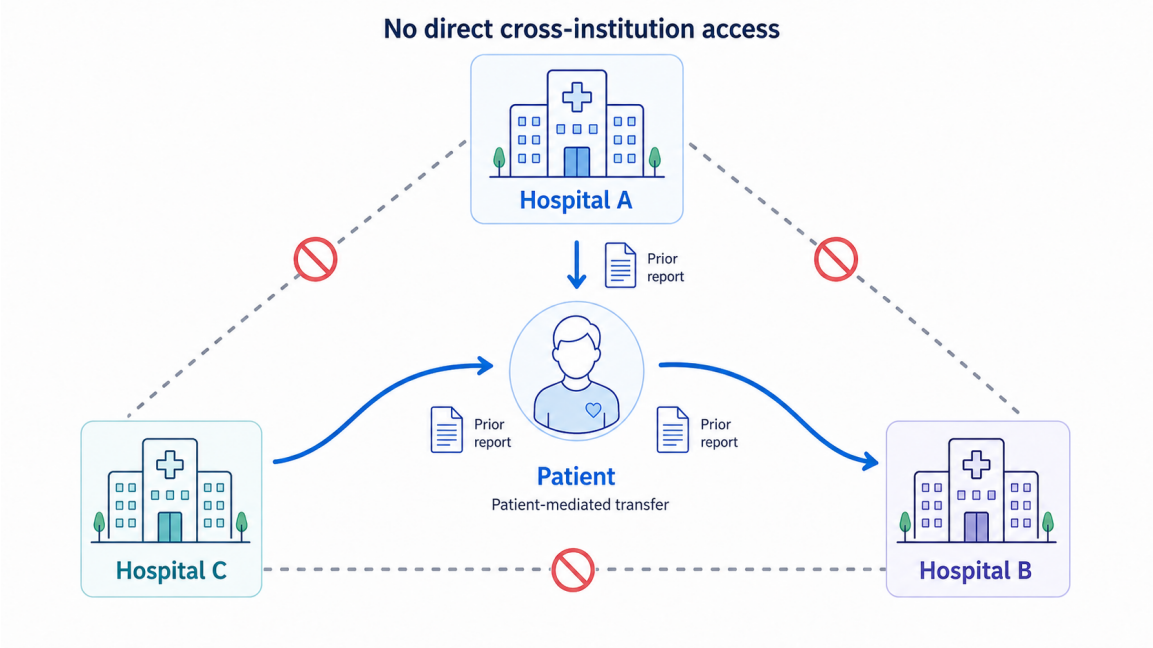

Figure 1: Cross-institution data silos in clinical document processing pipelines.

For clinicians, paper reports are inconvenient to read and cannot be integrated into EHR systems, limiting their usability for longitudinal review, structured retrieval Hossain et al. (2023), and clinical decision support. Even after applying OCR, the resulting text often remains difficult to interpret due to recognition errors, layout noise, and inconsistent formatting Li et al. (2024), and still lacks native compatibility with EHR schemas. From the patient perspective, the lack of a unified and structured electronic record makes it difficult to maintain a coherent view of medical history. This fragmentation hinders continuity of care, particularly for patients with complex or chronic diseases such as cancer. Together, these challenges highlight the need for systematic methods that can transform heterogeneous, OCR-derived clinical reports into structured, standardized representations suitable for EHR integration and continuity of patient care Walker et al. (2023). In practice, such an extraction layer can back-fill missing fields from outside reports into a receiving institution's EHR, assemble longitudinal timelines for chronic-disease or oncology follow-up, and expose report-derived criteria for clinical-trial eligibility screening. These are intended workflow uses, not claims that this study improves clinical decisions, trial enrolment, or patient outcomes.

Clinical reports often follow an explicit layout: clinical concepts appear as field headers (keys) followed by free-text content (values), separated by delimiters such as colons or layout cues Fu et al. (2020); Jaume et al. (2019). Figure 2 illustrates a typical patient admission report. This key–value structure is common across languages and across mixed-form clinical documents. Owing to wording differences across institutions, the same clinical concept may appear under different surface-form keys, yielding a highly variable and long-tailed key space in which previously unseen keys continue to emerge Wu et al. (2020).

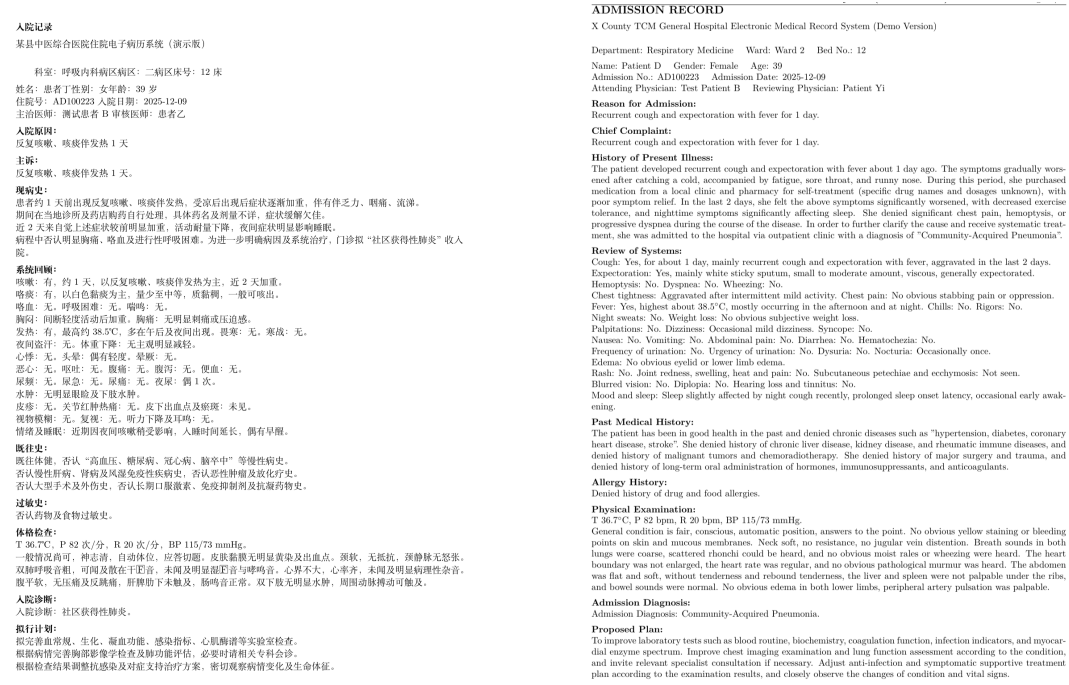

入院记录

某县中医综合医院住院电子病历系统（演示版）

科室：呼吸内科病区：二病区床号：12 床

姓名：患者丁性别：女年龄：39 岁
住院号：AD100223 入院日期：2025-12-09
主治医师：测试患者 B 审核医师：患者乙

入院原因：
反复咳嗽、咳痰伴发热 1 天

主诉：
反复咳嗽、咳痰伴发热 1 天。

现病史：
患者约 1 天前出现反复咳嗽、咳痰伴发热，受凉后出现症状逐渐加重，伴有伴乏力、咽痛、流涕。
期间在当地诊所及药店购药自行处理，具体药名及剂量不详，症状缓解欠佳。
近 2 天来自觉上述症状较前明显加重，活动耐量下降，夜间症状明显影响睡眠。
病程中否认明显胸痛、咯血及进行性呼吸困难。为进一步明确病因及系统治疗，门诊拟“社区获得性肺炎”收入院。

系统回顾：
咳嗽：有，约 1 天，以反复咳嗽、咳痰伴发热为主，近 2 天加重。
咯痰：有，以白色黏痰为主，量少至中等，质黏稠，一般可咳出。
咯血：无，呼吸困难：无，喘鸣：无。
胸闷：间断轻度活动后加重，胸痛：无明显刺痛或压迫感。
发热：有，最高约 38.5℃，多在午后及夜间出现，畏寒：无，寒战：无。
夜间盗汗：无，体重下降：无主观明显减轻。
心悸：无，头晕：偶有轻度，晕厥：无。
恶心：无，呕吐：无，腹痛：无，腹泻：无，便血：无。
尿频：无，尿急：无，尿痛：无，夜尿：偶 1 次。
水肿：无明显眼睑及下肢水肿。
皮疹：无，关节红肿热痛：无，皮下出血点及瘀斑：未见。
视物模糊：无，复视：无，听力下降及耳鸣：无。
情绪及睡眠：近期因夜间咳嗽稍受影响，入睡时间延长，偶有早醒。

既往史：
既往体健，否认“高血压、糖尿病、冠心病、脑卒中”等慢性病史。
否认慢性肝病、肾病及风湿免疫性疾病史，否认恶性肿瘤及放化疗史。
否认大型手术及外伤史，否认长期口服激素、免疫抑制剂及抗凝药物史。

过敏史：
否认药物及食物过敏史。

体格检查：
T 36.7℃，P 82 次/分，R 20 次/分，BP 115/73 mmHg。
一般情况尚可，神志清，自动体位，应答切题，皮肤黏膜无明显黄染及出血点。颈软，无抵抗，颈静脉无怒张。
双肺呼吸音粗，可闻及散在干罗音，未闻及明显湿罗音与哮鸣音，心界不大，心率齐，未闻及明显病理性杂音。
腹平软，无压痛及反跳痛，肝脾肋下未触及，肠鸣音正常。双下肢无明显水肿，周围动脉搏动可触及。

入院诊断：
入院诊断：社区获得性肺炎。

拟行计划：
拟完善血常规、生化、凝血功能、感染指标、心肌酶谱等实验室检查。
根据病情完善胸部影像学检查及肺功能评估，必要时请相关专科会诊。
根据检查结果调整抗感染及对症支持治疗方案，密切观察病情变化及生命体征。

ADMISSION RECORD

X County TCM General Hospital Electronic Medical Record System (Demo Version)

Department: Respiratory Medicine Ward: Ward 2 Bed No.: 12

Name: Patient D Gender: Female Age: 39
Admission No.: AD100223 Admission Date: 2025-12-09
Attending Physician: Test Patient B Reviewing Physician: Patient Yi

Reason for Admission:
Recurrent cough and expectoration with fever for 1 day.

Chief Complaint:
Recurrent cough and expectoration with fever for 1 day.

History of Present Illness:
The patient developed recurrent cough and expectoration with fever about 1 day ago. The symptoms gradually worsened after catching a cold, accompanied by fatigue, sore throat, and runny nose. During this period, she purchased medication from a local clinic and pharmacy for self-treatment (specific drug names and dosages unknown), with poor symptom relief. In the last 2 days, she felt the above symptoms significantly worsened, with decreased exercise tolerance, and nighttime symptoms significantly affecting sleep. She denied significant chest pain, hemoptysis, or progressive dyspnea during the course of the disease. In order to further clarify the cause and receive systematic treatment, she was admitted to the hospital via outpatient clinic with a diagnosis of "Community-Acquired Pneumonia".

Review of Systems:
Cough: Yes, for about 1 day, mainly recurrent cough and expectoration with fever, aggravated in the last 2 days.
Expectoration: Yes, mainly white sticky sputum, small to moderate amount, viscous, generally expectorated.
Hemoptysis: No. Dyspnea: No. Wheezing: No.
Chest tightness: Aggravated after intermittent mild activity. Chest pain: No obvious stabbing pain or oppression.
Fever: Yes, highest about 38.5°C, mostly occurring in the afternoon and at night. Chills: No. Rigors: No.
Night sweats: No. Weight loss: No obvious subjective weight loss.
Palpitations: No. Dizziness: Occasional mild dizziness. Syncope: No.
Nausea: No. Vomiting: No. Abdominal pain: No. Diarrhea: No. Hematochezia: No.
Frequency of urination: No. Urgency of urination: No. Dysuria: No. Nocturia: Occasionally once.
Edema: No obvious eyelid or lower limb edema.
Rash: No. Joint redness, swelling, heat and pain: No. Subcutaneous petechiae and ecchymosis: Not seen.
Blurred vision: No. Diplopia: No. Hearing loss and tinnitus: No.
Mood and sleep: Sleep slightly affected by night cough recently, prolonged sleep onset latency, occasional early awakening.

Past Medical History:
The patient has been in good health in the past and denied chronic diseases such as "hypertension, diabetes, coronary heart disease, stroke". She denied history of chronic liver disease, kidney disease, and rheumatic immune diseases, and denied history of malignant tumors and chemoradiotherapy. She denied history of major surgery and trauma, and denied history of long-term oral administration of hormones, immunosuppressants, and anticoagulants.

Allergy History:
Denied history of drug and food allergies.

Physical Examination:
T 36.7°C, P 82 bpm, R 20 bpm, BP 115/73 mmHg.
General condition is fair, conscious, automatic position, answers to the point. No obvious yellow staining or bleeding points on skin and mucous membranes. Neck soft, no resistance, no jugular vein distention. Breath sounds in both lungs were coarse, scattered rhonchi could be heard, and no obvious moist rales or wheezing were heard. The heart boundary was not enlarged, the heart rate was regular, and no obvious pathological murmur was heard. The abdomen was flat and soft, without tenderness and rebound tenderness, the liver and spleen were not palpable under the ribs, and bowel sounds were normal. No obvious edema in both lower limbs, peripheral artery pulsation was palpable.

Admission Diagnosis:
Admission Diagnosis: Community-Acquired Pneumonia.

Proposed Plan:
To improve laboratory tests such as blood routine, biochemistry, coagulation function, infection indicators, and myocardial enzyme spectrum. Improve chest imaging examination and lung function assessment according to the condition, and invite relevant specialist consultation if necessary. Adjust anti-infection and symptomatic supportive treatment plan according to the examination results, and closely observe the changes of condition and vital signs.

(a) The admission record in Chinese

(b) The English translation

Figure 2: A sample admission report and its English translation.

Table 1 shows examples of institution-specific surface-form variations for the same clinical keys in Chinese, together with their English translations. Even when the underlying clinical meaning is the same, different hospitals may use different section headers or expressions.

Figure 3 provides a real-world example of such variation for the key “Specialty Examination”. The three report snippets use different surface forms, all of which map to the canonical key “Specialty Examination”.

Treating field headers as queries and their contents as answers yields an extractive question answering (QA) formulation, but standard QA-based extractors assume a predefined, closed key set. Clinical report keys instead form an open and evolving space: surface forms vary across institutions and templates, and new forms continue to appear. Thus, inventory coverage limits the range of fields that a key-conditioned system can recover.

We address this problem with a canonical-key-conditioned extraction framework for semi-structured OCR clinical reports. The current inventory determines which fields are

Chinese		English	
Key	**Surface Forms**	**Key**	**Surface Forms**
既往史	既往病史，既往疾病，既往治疗史	Past Medical History	Past Illness History, Previous Diseases, Previous Treatment History
体格检查	查体所见，体检所见，体征情况	Physical Examination	Physical findings, Examination Findings, Clinical Signs
手术记录	手术经过，术中经过，手术过程，术中情况	Operative Record	Surgical Course, Intraoperative Course, Surgical Procedure, Intraoperative situation
专科检查	专科查体，专科检查所见，专科情况，专科查体所见	Specialty Examination	Specialty Physical Examination; Specialty Examination Findings; Specialty Status; Specialty Physical Examination Findings

Table 1: Examples of surface-form keys in Chinese clinical reports (and English translations).

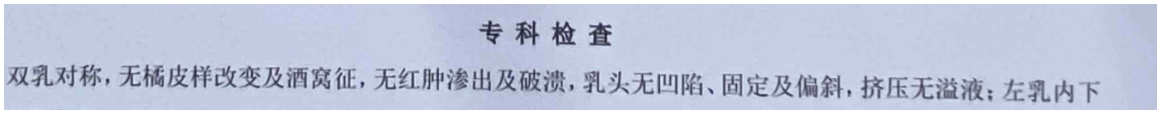

(a) Specialty Examination (专科检查)

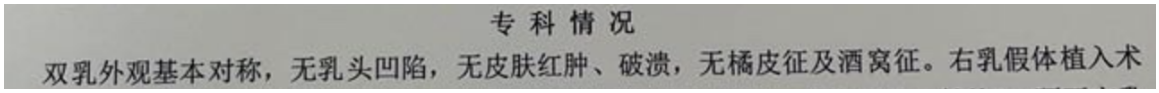

(b) Specialty Status (专科情况)

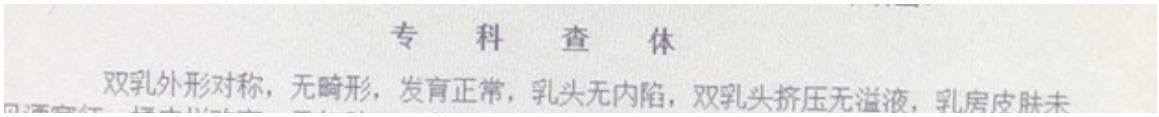

(c) Specialty Physical Examination (专科查体)

Figure 3: Examples of surface-form variants mapped to the canonical key "Specialty Examination".

queried, so inventory-external fields cannot enter the accepted output; normalization and iterative clustering maintain canonical keys and their aliases as new surface forms are reviewed. Our central experiment evaluates train-derived Top-N inventories and their corresponding models under a common architecture and fixed development set. By reporting coverage, conditional extraction, and end-to-end recovery separately, we distinguish the supported field range from value extraction once a field is supported. Gold-key-conditioned accuracy and efficiency comparisons therefore provide conditional rather than inventory-coverage evidence.

Generalizable Insights about Machine Learning in the Context of Healthcare

Canonical-key coverage is an explicit constraint on end-to-end field recovery. High conditional extraction accuracy cannot substitute for evaluating inventory coverage: when the canonical inventory does not represent valid surface forms or clinically relevant concepts, information present in the original report cannot enter the structured data. This can affect patient cohort construction, research analyses, and reuse of clinical information. Separating inventory coverage from conditional extraction performance therefore helps identify whether errors arise from the representation layer or the extraction model. This evaluation principle can also apply to other semi-structured document tasks in which heterogeneous surface forms must be mapped to a shared schema.

2. Related Work

Clinical document and OCR extraction. Transferred clinical records are often scanned or printed images that require OCR before their contents can be structured. OCR-derived clinical text contains character and layout noise that can impair downstream extraction Li et al. (2024). MedStruct-S extends this setting to semi-structured clinical reports with open-world keys and OCR noise Li et al. (2027), closely matching our focus on robust page-level span extraction.

Query-based field extraction. Question answering provides a practical formulation for extracting fields from clinical records with variable layouts. EMRQA established this paradigm for medical record extraction Pampari et al. (2018), and subsequent work has applied it to radiology reports Dada et al. (2024). Biomedical encoders including BioBERT Lee et al. (2019) and PubMedBERT Gu et al. (2021) support both QA and information-extraction settings.

Key normalization and open-world extraction. Semi-structured report keys vary across institutions and over time. This resembles biomedical entity normalization, which maps surface names to underlying concepts Liu et al. (2021), but here the normalized objects are report keys. In contrast to extraction methods that assume a fixed, known key set, we quantify the effect of incomplete inventories and use the result to guide inventory maintenance and expansion Lu et al. (2022); Shen et al. (2022).

3. Methodology

In our method, we treat each clinical-report page as the atomic unit of extraction. If a report contains multiple pages, we aggregate the page-level outputs.

3.1. Dataset and Annotation

We analyze a private corpus of oncology clinical-report images collected through a multi-institution oncology patient-management program, reflecting heterogeneity in clinical documentation and report templates. The corpus covers a diverse set of report categories, including outpatient medical records, biopsy pathology reports, examination records, post-operative pathology reports, genetic testing reports, admission records, and consultation

pathology reports. Among these, outpatient medical records are the most frequent category, accounting for approximately 35% of all reports.

All report images were digitized on premises with a privately deployed Baidu OCR V6 service (Baidu AI Cloud, 2025); no clinical image was sent to a public OCR endpoint. The extraction models consume only the page-level character sequence formed by concatenating recognized line strings in the engine-returned reading order; line/character confidence and geometry are stored as metadata and are not used as model inputs. Request parameters and response-normalization details are given in Appendix A.1.

To protect patient privacy, all personally identifiable information—including names, identification numbers, contact information, and addresses—was removed prior to annotation and replaced with a uniform placeholder symbol (**). Only de-identified OCR text was used in subsequent processing and analysis.

The corpus was annotated at the surface-form key–value (KV) pair level through a human-in-the-loop workflow. A locally deployed Qwen3-235B-A22B model (Yang et al., 2025) generated initial KV pre-annotations, which human reviewers corrected in Label Studio (Tkachenko et al., 2020–2025); unresolved cases were escalated for senior adjudication. The available records identify 29 distinct non-staff annotation accounts, but do not permit reliable inference about the number or clinical training of individual annotators. The recorded 430 human-hours refer to review and correction rather than annotation from scratch, corresponding to approximately 1.6 minutes per report or 11.7 seconds per KV pair. These are two normalizations of the same aggregate review time.

After exact full-OCR-text deduplication, 14,587 tasks were partitioned into 13,128 training tasks and 1,459 held-out tasks. These held-out tasks support the supplementary conditional-extraction and robustness analyses, whose shared evaluation set contains the 1,242 reports with valid reference spans (Appendix A.1). The Chinese coverage experiment instead used a fixed 7,639/849 train/development split from a distinct 8,488-report subset.

The distribution of surface-form keys exhibits a strong long-tailed pattern (Figure 4): a small set of frequent keys coexists with many rare surface forms. The denominator and split provenance required to report exact cumulative coverage thresholds have not been verified; we therefore omit those values.

Algorithm 1: Iterative Canonical Key Expansion and Key–Value Extraction

Require: Initial canonical key set $\mathcal{K}_{\mathrm{c}}^{(0)}$, initial alias mapping $\mathcal{K}_{\mathrm{a}}^{(0)}$, clinical report batches $\{\mathcal{D}_b\}_{b=1}^{T}$

Ensure: Canonicalized key–value pairs $\mathcal{S}_{\mathrm{c}}$

Initialize QA models QA_{v} and QA_{k} using augmented data
$\mathcal{K}_{\mathrm{c}} \leftarrow \mathcal{K}_{\mathrm{c}}^{(0)}$, $\mathcal{K}_{\mathrm{a}} \leftarrow \mathcal{K}_{\mathrm{a}}^{(0)}$
for $b = 1$ **to** T **do**
  Observe new report batch $\mathcal{D}_b$
  Initialize observed key set $\mathcal{K}(\mathcal{D}_b) \leftarrow \emptyset$
  for each report page with OCR text $\mathcal{T} \in \mathcal{D}_b$ **do**
    for each canonical key $kc \in \mathcal{K}_{\mathrm{c}}$ **do**
      Query value: $v_{kc} \leftarrow \mathrm{QA}_{\mathrm{v}}(q_{\mathrm{v}}(kc), \mathcal{T})$
      Query surface-form key: $k_{kc} \leftarrow \mathrm{QA}_{\mathrm{k}}(q_{\mathrm{k}}(kc), \mathcal{T})$
      if $k_{kc} \neq \emptyset$ **then**
        $\mathcal{K}(\mathcal{D}_b) \leftarrow \mathcal{K}(\mathcal{D}_b) \cup \{k_{kc}\}$
        Add (k_{kc}, v_{kc}) to $\mathcal{S}_{\mathrm{c}}$
      end if
    end for
  end for
  Identify novel surface-form keys: $\mathcal{K}_{\mathrm{new}} \leftarrow \mathcal{K}(\mathcal{D}_b) \setminus \left(\mathcal{K}_{\mathrm{c}} \cup \bigcup_{kc \in \mathcal{K}_{\mathrm{c}}} \mathcal{K}_{\mathrm{a}}(kc)\right)$
  Format and clean $\mathcal{K}_{\mathrm{new}}$
  Canonicalize $\mathcal{K}_{\mathrm{new}}$ via embedding-based clustering with human verification
  Update canonical key set $\mathcal{K}_{\mathrm{c}}$ and alias mapping $\mathcal{K}_{\mathrm{a}}$
  Fine-tune QA models with expanded $\mathcal{K}_{\mathrm{c}}$ and $\mathcal{K}_{\mathrm{a}}$
end for
return $\mathcal{S}_{\mathrm{c}}$

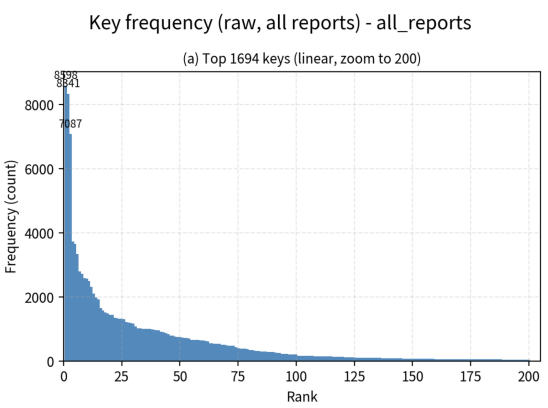

(a) Rank–frequency plot (top-200, linear scale)

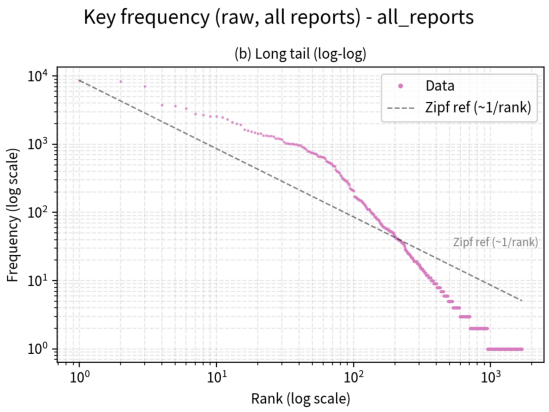

(b) Log–log rank–frequency plot with a Zipf reference

Figure 4: Rank–frequency characteristics of surface-form key expressions in the full corpus.

3.2. Problem Formulation

We represent the OCR-derived text of a clinical report page as an ordered sequence of characters, denoted by

$$\mathcal{T} = \big(c_1, c_2, \cdots, c_M\big),$$

where M is the total number of OCR characters in the page, and the order of characters preserves the original reading order of the document.

Let $\mathcal{K}^\star$ denote the latent universe of all possible keys that may appear in real-world clinical reports and let $\mathcal{K}$ denote the set of all annotated keys collected during the labeling process. Note that $\mathcal{K}^\star$ cannot be fully observed in practice. That is, $\mathcal{K} \subset \mathcal{K}^\star$. The keys in $\mathcal{K}$ may include lexical variants or synonyms that correspond to the same underlying semantic meaning. We introduce a canonical key space:

$$\mathcal{K}_{\mathrm{c}} = \{kc_1, kc_2, \cdots, kc_{\mathrm{K}}\},$$
where K is the number of observed canonical keys.

We define an alias set for each observed canonical key as: $\mathcal{K}_{\mathrm{a}}(kc) \subseteq \mathcal{K}$, where all elements in $\mathcal{K}_{\mathrm{a}}(kc)$ are semantically equivalent to kc, and kc is not in the set of $\mathcal{K}_{\mathrm{a}}(kc)$. The observed space $\mathcal{K}$ is the union of all alias sets and canonical sets:

$$\mathcal{K} = \mathcal{K}_{\mathrm{c}} \ \cup \bigcup_{kc \in \mathcal{K}_{\mathrm{c}}} \mathcal{K}_{\mathrm{a}}(kc).$$

We define a key canonicalization function:

$$\psi : \mathcal{K} \to \mathcal{K}_{\mathrm{c}},$$

such that:

$$\psi(k) = kc \quad \text{if and only if} \quad k \in \mathcal{K}_{\mathrm{a}}(kc) \cup \{kc\}.$$

This mapping function collapses synonymous keys into a single canonical representation. During inventory expansion, newly discovered surface-form keys are formatted, semantically clustered, and reviewed before being added to the canonical inventory. Under the documented review protocol, annotators confirm proposed canonical merges, manually split a proposed cluster when it mixes distinct field semantics, and route unresolved assignments to senior review; the senior ruling governs the final canonical-key and alias decision.

Let $k \in \mathcal{K}$ denote a surface-form key observed in a report, v denote its value, and $\mathcal{V}$ denote the value set that may appear in the real-world clinical reports. Thus, the key–value pair is represented by (k, v). The canonical key–value pair is represented by:

$$\big(\psi(k), v\big) \in \mathcal{K}_{\mathrm{c}} \times \mathcal{V}.$$

For the purpose of formulation, we first assume that an incomplete but known canonical key set is provided as prior knowledge. There are two steps in extracting the key–value pairs. First, we formulate value extraction as a QA task conditioned on canonical keys. The query denoted by $q_{\mathrm{v}}(kc)$ represents the question conditioned on a canonical key. A BERT-based QA model is then applied to the OCR token sequence:

$$\mathrm{QA}_{\mathrm{v}} : \big(q_{\mathrm{v}}(kc), \mathcal{T}\big) \ \mapsto \ v_{kc} \in \mathcal{V} \cup \{\emptyset\}. \tag{1}$$

The output v_{kc} denotes the extracted value corresponding to a canonical key or $\emptyset$ if no value is found. The output key–value space is given by:

$$\mathcal{S}_{\mathrm{c}} = \big\{(kc, v_{kc}) \;\big|\; kc \in \mathcal{K}_{\mathrm{c}},\ v_{kc} \neq \emptyset\big\}.$$

For any canonical key, kc_i, the simplest prompt for the QA task is:
`Extract the value of the key` kc_i.
To help the model recognize synonymous surface forms, the query may include some or all known aliases of the canonical key:

> `Extract the value of the key` kc_i`. The key in the text may be a variant of the canonical key, such as` $ka_1, ka_2, \ldots$.

where $ka_1, ka_2, \ldots \in \mathcal{K}_{\mathrm{a}}(kc_i)$.

Secondly, we identify the surface-form alias of each canonical key as it appears in the original OCR text. Using the same BERT-based QA model, we pose a second query for each canonical key: $q_{\mathrm{k}}(kc)$. Formally:

$$\mathrm{QA}_{\mathrm{k}} : \big(q_{\mathrm{k}}(kc), \mathcal{T}\big) \;\mapsto\; k_{kc} \in \mathcal{K} \cup \{\emptyset\}. \tag{2}$$

The output k_{kc} denotes the original key observed on the page or $\emptyset$ if no alias is present.

Note that the example prompt is illustrated in English. In our implementation, its equivalent Chinese version is adopted. Combining Eqs. (1) and (2) yields (k_{kc}, v_{kc}).

In practice, neither the canonical inventory $\mathcal{K}_{\mathrm{c}}$ nor the alias mapping $\mathcal{K}_{\mathrm{a}}$ is available as prior knowledge. Given a report corpus that grows as successive batches $\{\mathcal{D}_b\}_{b=1}^{T}$, newly observed surface-form keys expand the observed key space over time, so key mining and canonicalization are treated as an iterative process rather than one-time preprocessing. In the expansion step of Fig. 5, the LLM component is a locally deployed Qwen3-235B-A22B model (Yang et al., 2025), which generates candidate New Surface Key Forms from each incoming report batch. These candidates are formatted and cleaned, embedded with BGE-large-zh-v1.5, and grouped using average-linkage clustering with cosine distance threshold 0.25. The threshold is selected from a silhouette sweep, and the documented human-review rules above are applied before the canonical inventory and alias mapping are updated. BGE is used in this canonicalization stage, not for candidate surface-key identification or KV pre-annotation. The downstream QA models are then updated with the expanded inventory. With a document length L and K available canonical keys, inference requires K key-conditioned queries and scales as $O(LK)$. This cost is the implementation trade-off that makes the inventory an explicit gate on supported fields.

3.3. Evaluation Method

Exact span matching is the primary metric. We additionally report BTM-3 to distinguish small punctuation- or whitespace-boundary differences from larger extraction errors. Before comparison, both strings undergo the same deterministic normalization $\nu(\cdot)$: Unicode NFKC normalization, dash unification, edge-whitespace removal, and removal of common

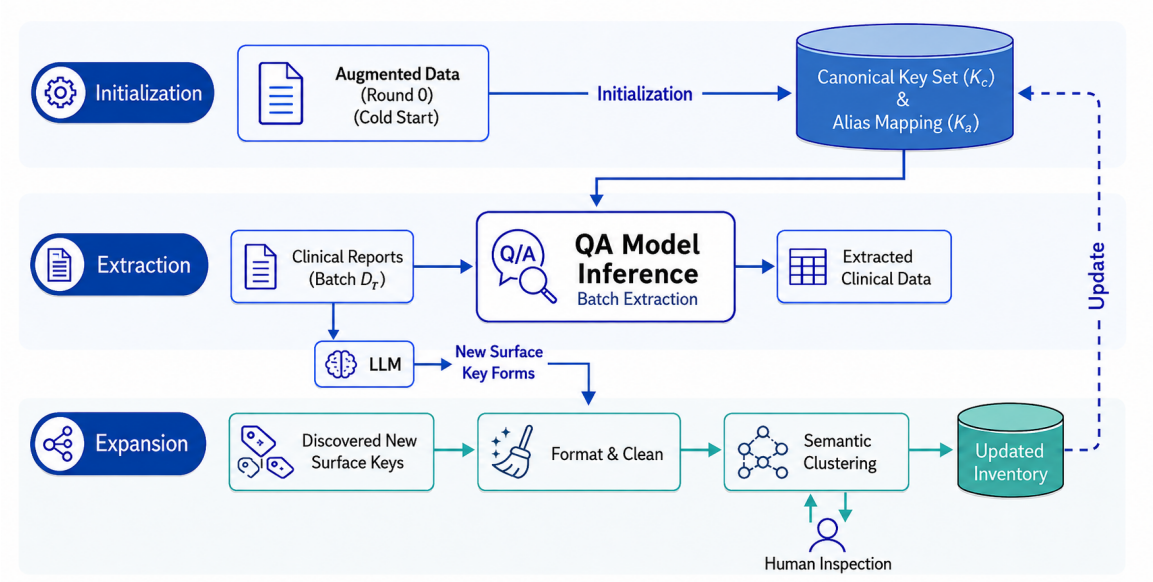

Figure 5: Overview of the proposed iterative pipeline

punctuation at the two string boundaries. Exact matching then requires equality after normalization between a predicted value $\hat{v}$ and its gold value v:

$$\text{Exact}(\hat{v}, v) = \begin{cases} 1, & \text{if } \nu(\hat{v}) = \nu(v), \\ 0, & \text{otherwise.} \end{cases}$$

The second criterion is BTM-3, a boundary-tolerant match that applies an Edge-3 boundary rule. Let $\tau_3(\cdot)$ remove at most three characters in total from the two boundaries when those characters are whitespace or punctuation. We compute

$$\text{BTM-3}(\hat{v}, v) = \begin{cases} 1, & \text{if } \nu(\tau_3(\hat{v})) = \nu(\tau_3(v)), \\ 0, & \text{otherwise.} \end{cases}$$

This criterion tolerates small boundary artifacts without granting partial credit for an arbitrary interior mismatch. Text-overlap matching, defined by substring containment after normalization, is reported only as a diagnostic.

Under both criteria, we report precision, recall, and F1 conditioned on canonical keys.

To assess overall system performance, we further compute precision, recall, and F1 over surface-form key–value pairs, where a prediction is considered correct only if both the surface-form key and its associated value are correctly extracted under the specified matching criterion.

Key coverage quantifies the proportion of gold field instances supported by the current canonical inventory. For a fixed evaluation set of gold key–value instances G and an available inventory $\widehat{\mathcal{K}}_c$, let

$$G_{\text{cov}} = \{(k, v) \in G : \psi(k) \in \widehat{\mathcal{K}}_c\}, \qquad C_{\text{instance}} = \frac{|G_{\text{cov}}|}{|G|}. \tag{3}$$

This instance-weighted definition is tied to a named corpus, split, inventory version, and train-only ranking; it does not estimate the unobservable universe of all possible clinical keys. We separately report conditional recall on supported instances,

$$R_{\text{conditional}} = \frac{\text{TP}}{|G_{\text{cov}}|}, \tag{4}$$

and end-to-end recall on all gold instances,

$$R_{\text{end-to-end}} = \frac{\text{TP}}{|G|}. \tag{5}$$

Because the QA system queries only inventory members, unsupported fields cannot enter its accepted output. Under the same pooled-micro matching universe, the recall identity $R_{\text{end-to-end}} = C_{\text{instance}} R_{\text{conditional}}$ therefore holds. It is a recall decomposition, not a Precision or F1 decomposition. In the remainder of the paper we refer to C_{instance} as instance coverage, $R_{\text{conditional}}$ as conditional recall, and $R_{\text{end-to-end}}$ as end-to-end recall.

3.4. Training Method

The Chinese coverage experiment uses BERT-based extractive QA models with token-level start and end heads. Each Top-N inventory is ranked from the 7,639 training reports only and paired with its corresponding model; all conditions are evaluated on the same 849-report development set. During inference, only canonical keys in the selected inventory are queried, and the resulting surface-form keys and values are assembled into accepted key–value pairs.

Long documents are handled separately in the two implementations. The primary BERT-based QA experiment uses a 512-token question–context window and adapts the context budget to the query length. It processes non-overlapping, blank-line-delimited segments and aggregates predictions for each report–key query; it neither uses a sliding overlap nor reconnects spans across segments. The supplementary BERT–BiLSTM–CRF implementation instead uses overlapping chunks, as specified in Appendix A.1. We report pooled-micro Exact and BTM-3 precision, recall, and F1 over gold and accepted predicted report–key units; Overlap is reported only as a separately labelled diagnostic.

The conditional extraction comparison uses a separate protocol on content-deduplicated data. Models are restricted to the same gold key universe and evaluate conditional value extraction rather than the inventory-gated end-to-end mechanism studied in the Chinese coverage experiment. The complete split, filtering, seed, model, and decoding contracts are listed in Appendix A.1.

4. Results

4.1. Canonical Inventory and Iterative Expansion

On the valid pre-deduplication annotation snapshot, canonicalization maps 2,394 observed surface-form keys to 1,339 canonical keys, a 44.1% reduction in distinct key labels. This statistic describes lexical consolidation rather than compression of reports, key–value instances, or storage. Figure 6 summarizes the resulting cluster-size distribution.

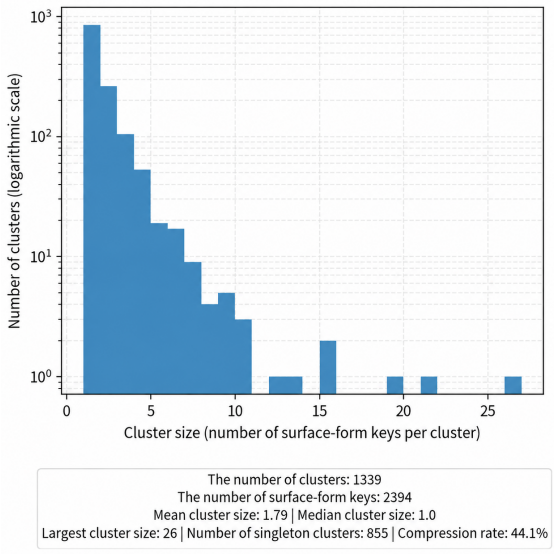

(a) Number of clusters by cluster size

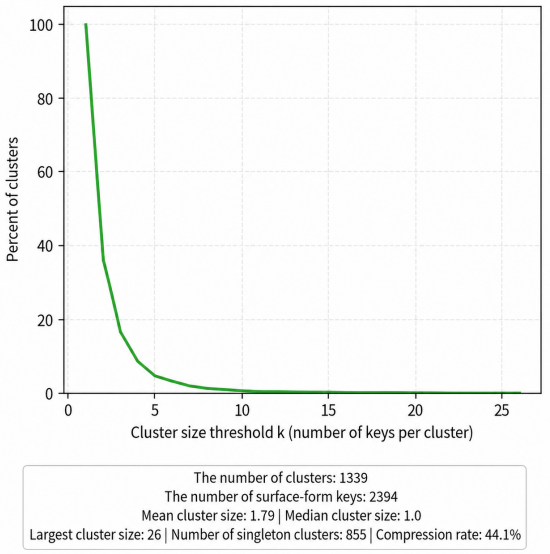

(b) Complementary cumulative distribution function of cluster sizes

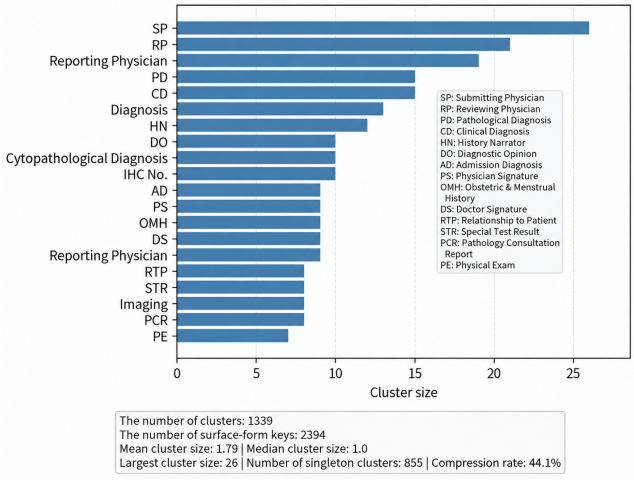

(c) Sizes of the top 20 largest clusters

Figure 6: Canonicalization clustering statistics of surface-form keys.

The mean cluster size is 1.79, the largest cluster contains 26 surface forms, and 855 observed keys occur only once. These statistics illustrate both substantial alias redundancy and a long tail of institution-specific expressions. On the 536 surface keys shared by the iterative and one-shot assignments, V-measure was 0.9331, indicating that incremental updating preserved a similar grouping structure on the shared key set; additional consistency metrics are reported in Appendix A.4. This comparison did not test downstream extraction or human workload relative to one-shot clustering.

Table 2: Chinese instance coverage and pooled-micro Exact extraction across train-derived inventories.

Inventory	Coverage	Conditional			End-to-end		
		P	R	F1	P	R	F1
Top-10	0.4019	0.8919	0.8794	0.8856	0.8919	0.3534	0.5062
Top-20	0.5591	0.8647	0.8704	0.8675	0.8647	0.4866	0.6228
Top-50	0.8233	0.8616	0.8653	0.8634	0.8616	0.7124	0.7799
Top-80	0.9197	0.8490	0.8535	0.8513	0.8490	0.7850	0.8158
Top-90	0.9339	0.8361	0.8571	0.8464	0.8361	0.8004	0.8179
Top-95	0.9406	0.8365	0.8615	0.8488	0.8365	0.8103	0.8232
Top-100	0.9465	0.8265	0.8497	0.8379	0.8265	0.8042	0.8152

4.2. Chinese Coverage and End-to-End Recovery

We evaluated seven train-derived inventories (Top-10 through Top-100) on the same 849-report development set. Each inventory was ranked from 7,639 training reports and used to constrain the corresponding key-conditioned extraction model at inference. We report instance coverage together with pooled-micro conditional and inventory- constrained end-to-end precision, recall, and F1, separating the fields that the inventory supports from the accuracy of extracting those fields.

Table 2 shows that expanding the inventory raises fixed-development instance coverage from 0.4019 at Top-10 to 0.9465 at Top-100. Over the same range, conditional Exact F1 decreases from 0.8856 to 0.8379, whereas inventory-constrained end-to-end recall rises from 0.3534 to 0.8042. End-to-end Exact F1 reaches 0.8232 at Top-95 and then decreases to 0.8152 at Top-100. Thus, in this corpus and protocol, inventory expansion substantially broadens recoverable fields, while later additions exhibit diminishing and non-monotone gains as conditional extraction becomes harder.

4.3. Supplementary Experiments

We compared BERT–BiLSTM–CRF with LoRA-adapted Qwen3 models (Yang et al., 2025; Hu et al., 2022) on a separate held-out set of 1,242 content-deduplicated reports. All models received the gold canonical key for each query and extracted only the corresponding value. Qwen3-0.6B and Qwen3-1.7B achieved slightly higher Exact F1, whereas BERT required substantially less inference time on the same device. This comparison concerns conditional extraction, not open-world coverage.

On the official DocILE (Šimsa et al., 2023) split, expanding a train-derived inventory from Top-5 to Top-20 increases validation instance coverage from 45.40% to 88.71% and the number of exactly recovered fields from 1,540 to 2,919, while conditional Exact extraction decreases from 0.8271 to 0.8024. This provides external evidence for the coverage–recovery mechanism in a public English document domain, rather than evidence of transfer to English clinical reports. Under controlled synthetic character corruption, the BERT–BiLSTM–CRF model's Exact F1 decreases from 0.9060 at 0% target character error rate (CER) to 0.1398 at 20%; this is a stress test, not a measured production OCR error distribution.

In an independent structured-representation study, adding structured fields to raw text produced task-dependent effects: accuracy increased by 3.27 percentage points for histologic grade and 3.52 points for treatment response, showed no clear improvement for stage, recurrence, or primary site, and decreased by 5.54 points for 5-year survival. Because these fields were generated separately by a private deployment of DeepSeek-V4-Flash (DeepSeek-AI, 2026), this experiment evaluates the downstream utility of an explicit structured representation rather than the external validity of our extractor.

5. Conclusion

We study the clinically important problem of extracting header–content fields from heterogeneous OCR clinical reports. We introduce an iterative canonical-key-conditioned extraction pipeline that combines surface-key mining, alias mapping, canonical inventory expansion, and incremental human verification.

Inventory expansion improved end-to-end recall, but F1 gains diminished and became non-monotone in the tail. The appropriate Top-N operating point is corpus- and protocol-specific rather than a universal constant.

Limitations. The primary corpus reflects one oncology patient-management setting. Because the archive lacks independent pre-adjudication annotations, we report a stratified retrospective revision audit rather than formal inter-annotator agreement. OCR robustness was assessed with controlled synthetic corruption, not production reports with paired human transcriptions. Accordingly, the numerical operating points are corpus- and protocol-specific; within the evaluated setting, canonical-key coverage remains an explicit constraint on end-to-end field recovery.

Implementation Availability

Sanitized implementation materials are available in the fixed release `v0.1.0-camera-ready`: github.com/AI-Starfish-Research/Key-Coverage-Matters/tree/v0.1.0-camera-ready

The repository contains code, configuration templates, synthetic examples, and reviewed field-label-only canonical-inventory and alias snapshots. Clinical-report images, OCR text, annotation exports, predictions, and checkpoints are not publicly released.

References

Baidu AI Cloud. Baidu ocr technical documentation. https://ai.baidu.com/tech/ocr, 2025. Accessed: 2025.

Amin Dada, Tim Leon Ufer, Moon Kim, Max Hasin, Nicola Spieker, Michael Forsting, Felix Nensa, Jan Egger, and Jens Kleesiek. Information extraction from weakly structured radiological reports with natural language queries. *European Radiology*, 34(1):330–337, 2024.

DeepSeek-AI. Deepseek-v4: Towards highly efficient million-token context intelligence, 2026. URL https://arxiv.org/abs/2606.19348.

Sunyang Fu, David Chen, Huan He, Sijia Liu, Sungrim Moon, et al. Clinical concept extraction: A methodology review. *Journal of Biomedical Informatics*, 2020.

Yu Gu, Robert Tinn, Hao Cheng, Michael Lucas, Naoto Usuyama, Xiaodong Liu, Tristan Naumann, Jianfeng Gao, and Hoifung Poon. Domain-specific language model pretraining for biomedical natural language processing. *ACM Transactions on Computing for Healthcare*, 2021.

Elias Hossain, Rajib Rana, Niall Higgins, Jeffrey Soar, Prabal Datta Barua, Anthony R. Pisani, and Kathryn Turner. Natural language processing in electronic health records in relation to healthcare decision-making: A systematic review. *Computers in Biology and Medicine*, 2023.

Edward J. Hu, Yelong Shen, Phillip Wallis, Zeyuan Allen-Zhu, Yuanzhi Li, Shean Wang, Lu Wang, and Weizhu Chen. LoRA: Low-rank adaptation of large language models. In *International Conference on Learning Representations*, 2022. URL https://openreview.net/forum?id=nZeVKeeFYf9.

Guillaume Jaume, Hazım Kemal Ekenel, and Jean-Philippe Thiran. Funsd: A dataset for form understanding in noisy scanned documents. In *Proceedings of the 2019 International Conference on Document Analysis and Recognition Workshops (ICDARW)*, volume 2, pages 1–6. IEEE, 2019.

Jinhyuk Lee, Wonjin Yoon, Sungdong Kim, Donghyeon Kim, Sunkyu Kim, Chan Ho So, and Jaewoo Kang. Biobert: a pre-trained biomedical language representation model for biomedical text mining. *Bioinformatics (Oxford, England)*, 36(4):1234–1240, 2019. doi: 10.1093/bioinformatics/btz682.

Yiming Li, Qiang Wei, Xinghan Chen, Jianfu Li, Cui Tao, and Hua Xu. Improving tabular data extraction in scanned laboratory reports using deep learning models. *Journal of Biomedical Informatics*, 159:104735, 2024.

Yingyun Li, Yu Wang, and Haiyang Qian. Medstruct-s: A benchmark for key discovery, key-conditioned qa and semi-structured extraction from ocr clinical reports. In *Knowledge Science, Engineering and Management*, volume 16636 of *Lecture Notes in Computer Science*, pages 131–141. Springer, 2027. doi: 10.1007/978-981-92-2864-5_12.

Fangyu Liu, Ehsan Shareghi, Zaiqiao Meng, Marco Basaldella, and Nigel Collier. Self-alignment pretraining for biomedical entity representations. In *Proceedings of the 2021 conference of the North American chapter of the association for computational linguistics: human language technologies*, pages 4228–4238, 2021.

Yaojie Lu, Qing Liu, Dai Dai, Xinyan Xiao, Hongyu Lin, Xianpei Han, Le Sun, and Hua Wu. Unified structure generation for universal information extraction. In *Proceedings of the 60th Annual Meeting of the Association for Computational Linguistics (Volume 1: Long Papers)*, pages 5755–5772, Dublin, Ireland, May 2022. Association for Computational Linguistics. doi: 10.18653/v1/2022.acl-long.395. URL https://aclanthology.org/2022.acl-long.395/.

Anusri Pampari, Preethi Raghavan, Jennifer J. Liang, and Jian Peng. emrqa: A large corpus for question answering on electronic medical records. In *Proceedings of the 2018 Conference on Empirical Methods in Natural Language Processing (EMNLP)*, 2018.

Yongliang Shen, Xiaobin Wang, Zeqi Tan, Guangwei Xu, Pengjun Xie, Fei Huang, Weiming Lu, and Yueting Zhuang. Parallel instance query network for named entity recognition. In *Proceedings of the 60th Annual Meeting of the Association for Computational Linguistics (Volume 1: Long Papers)*, pages 947–961, Dublin, Ireland, May 2022. Association for Computational Linguistics. doi: 10.18653/v1/2022.acl-long.67. URL https://aclanthology.org/2022.acl-long.67/.

Maxim Tkachenko, Mikhail Malyuk, Andrey Holmanyuk, and Nikolai Liubimov. Label Studio: Data labeling software. https://github.com/HumanSignal/label-studio, 2020–2025. Open-source software.

Štěpán Šimsa, Milan Šulc, Michal Uřičář, Yash Patel, Ahmed Hamdi, Matěj Kocián, Matyáš Skalický, Jiří Matas, Antoine Doucet, Mickaël Coustaty, and Dimosthenis Karatzas. DocILE benchmark for document information localization and extraction. *arXiv preprint arXiv:2302.05658*, 2023. URL https://arxiv.org/abs/2302.05658.

Douglas M Walker, William L Tarver, Prasad Jonnalagadda, Lindsay Ranbom, Eric W Ford, and Sudeep Rahurkar. Perspectives on challenges and opportunities for interoperability: Findings from key informant interviews with stakeholders in ohio. *JMIR Medical Informatics*, 11:e43848, 2023.

Stephen Wu, Kirk Roberts, Sagnik Datta, et al. Deep learning in clinical natural language processing: a methodical review. *Journal of the American Medical Informatics Association*, 27(3):457–470, 2020.

An Yang, Anfeng Li, Baosong Yang, Beichen Zhang, Binyuan Hui, et al. Qwen3 technical report. *arXiv preprint arXiv:2505.09388*, 2025. URL https://arxiv.org/abs/2505.09388.

Appendix A. Supplementary Experiments and Implementation Details

A.1. Reproducibility protocol

OCR preprocessing. Clinical-report images were processed page by page by a privately deployed Baidu OCR V6 service (Baidu AI Cloud, 2025). Each request sent one page image as base64-encoded content. The service used Chinese–English general text recognition with page-direction detection and returned line- and character-level text, confidence, and locations.

The response was normalized to line-level records containing recognized text, rectangular location, and confidence; character records retained text, location, and confidence when available. The model input concatenated line text in service-returned order, while confidence and geometry remained metadata; multi-page outputs were aggregated after extraction. This production configuration is distinct from the synthetic corruption stress test in Table 10.

Long-document handling. Table 3 distinguishes the query-conditioned budget splitting used for Chinese coverage from the sliding-window and span-merging path used for conditional extraction. The latter's 50-token overlap and span reconnection do not apply to the Chinese coverage results.

Table 3: Long-document handling in the Chinese coverage experiment and the conditional extraction comparison.

Setting	Chinese coverage experiment	Conditional extraction comparison
Input limit	512 tokens for the question–context pair	512 tokens
Nominal context/chunk size	$\min(500, 512 - \lvert q \rvert - 3)$ tokens for query q (nominal 500)	500 tokens
Segmentation	Blank-line-delimited line segments; greedy budget splitting only when needed	Token sliding windows
Overlap / stride	None	50-token overlap / 450-token stride
Truncation fallback	Re-split the affected candidate greedily at 80% of its context budget; drop only a subchunk that still cannot be encoded	Each window is independently encoded within the 512-token limit
Cross-chunk aggregation	Per report–key query, select the maximum null score across chunks; no cross-chunk span concatenation	Convert local spans to report-level character offsets; remove duplicate (type, s, e) spans; merge same-type overlapping or adjacent spans with gap ≤ 5, then recover text from the full report

Corpus snapshots. Table 4 lists the data snapshots. Chinese coverage uses a separate 8,488-report cohort.

Table 4: Corpus snapshots and evaluation sets.

Snapshot	Count	Definition and use
Collected reports	16,144	Pre-validity-screen census; acquisition and total-time reference only.
Valid annotation tasks	15,991	After 153 reports failed the validity screen; contains 132,798 KV pairs and 2,394 surface-form keys.
Deduplicated task pool	14,587	Exact full-OCR-text deduplication removed 1,404 tasks.
Seed-42 task partition	13,128 / 1,459	Training / held-out split of the deduplicated pool.
Held-out evaluation set	1,458	One split task had no evaluation record; used for conditional evaluation and timing.
Common evaluation subset	1,242	Held-out reports with valid gold spans; the 216 excluded reports lacked a valid span.

Retrospective revision audit. To characterize annotation stability in the retained archive, we searched the Label Studio PostgreSQL database, two SQLite snapshots, and 47 historical exports. These sources did not recover demonstrably independent, blinded, pre-adjudication annotation pairs, so formal inter-annotator agreement cannot be computed. We therefore sampled 200 reports (40 from each of five report categories) and compared the earliest and final retained versions of the same annotation record. Table 5 reports exact span or relation F1 and the proportion of unchanged reports. It measures revision stability, not independent inter-annotator agreement. Across the five equally sized strata, KEY exact-span F1 ranged from 0.9228 to 0.9619 and VALUE exact-span F1 from 0.9167 to 0.9552.

Table 5: Revision stability between the earliest and final retained versions of the same annotation record (200 reports).

Outcome	Estimate
KEY exact span-F1	0.9473
VALUE exact span-F1	0.9424
HOSPITAL exact span-F1	0.9776
KEY→VALUE relation-F1	0.9598
Unchanged reports	37.0%

Evaluation and inference settings. Table 6 contrasts the two primary protocols.

Table 6: Core evaluation protocols.

Setting	Chinese coverage	Conditional extraction
Snapshot and split	8,488 reports; seed-42 7,639/849 train/development split	14,587 deduplicated tasks; seed-42 13,128/1,459 train/held-out split
Duplicate handling	None	Exact full-OCR-text deduplication before splitting
Key condition	Training-ranked Top-N inventories (10, 20, 50, 80, 90, 95, 100); canonical-key queries	Gold canonical keys; Qwen receives the gold key list, and CRF predictions are mapped to the same canonical set
Evaluation population	All 849 development reports at each Top-N	1,458 held-out reports; 1,242 common reports with valid gold spans
Metrics	Micro Exact and BTM-3 P/R/F1; Overlap diagnostic; conditional and end-to-end recovery separate	Micro Exact and BTM-3 P/R/F1 on the common subset; Overlap diagnostic

Inference settings. Chinese coverage uses archived checkpoints and deterministic rescoring; its original training configuration was not retained. Multilingual BERT extractive QA uses 512-token question–context pairs (500-token context), batch size 1, query templates, and a 0.5 no-answer threshold; each Top-N inventory uses its matching model. The BERT–BiLSTM–CRF baseline uses a three-layer BiLSTM (hidden size 384), CRF, and BIOE labels; it trains for six epochs (batch size 8, learning rate 2×10^{-5}, weight decay 0.03, warm-up ratio 0.05, dropout 0.2, and gradient clipping 1.0) and evaluates with batch size 16 and 500/50 chunk aggregation. Qwen3-0.6B/1.7B use the LoRA SFT configuration in Table 9 and greedy chat decoding (at most 2,048 new tokens; batch size 1; seed 42). Qwen3-32B uses one worked example and the gold key list per record with greedy decoding (at most 2,048 new tokens; batch size 8; seed 42).

A.2. Supplementary Chinese coverage results

Table 7 provides the boundary-tolerant results for the 849-report development set. All inventory-gate violation counts and pooled-recall residuals are zero.

Table 7: Boundary-tolerant Chinese coverage results under the Chinese coverage experiment.

Inventory	Coverage	Conditional			End-to-end		
		P	R	F1	P	R	F1
Top-10	0.4019	0.8919	0.8794	0.8856	0.8919	0.3534	0.5062
Top-20	0.5591	0.8642	0.8700	0.8671	0.8642	0.4864	0.6224
Top-50	0.8233	0.8613	0.8651	0.8632	0.8613	0.7122	0.7797
Top-80	0.9197	0.8490	0.8535	0.8513	0.8490	0.7850	0.8158
Top-90	0.9339	0.8358	0.8568	0.8462	0.8358	0.8002	0.8176
Top-95	0.9406	0.8366	0.8616	0.8489	0.8366	0.8104	0.8233
Top-100	0.9465	0.8265	0.8497	0.8379	0.8265	0.8042	0.8152

A.3. Conditional extraction baselines

Table 8 compares three models on the same 1,242-report subset. Gold canonical keys are supplied, so this is a conditional extraction comparison rather than end-to-end recovery; timing and memory were measured on one NVIDIA RTX 4090.

Model	Exact F1	BTM-3 F1	Overlap F1	Batch	Time (s)	Peak VRAM
BERT–BiLSTM–CRF 0.2B	0.90606	0.90643	0.97170	16	65.58	5,120 MiB
Qwen3-0.6B LoRA	0.92023	0.92994	0.96098	1	6,155.24	5,892 MiB
Qwen3-1.7B LoRA	0.92011	0.92889	0.96090	1	6,346.02	8,140 MiB

Table 8: Gold-key-conditioned extraction accuracy on the common evaluation subset of 1,242 reports. Time and peak VRAM denote full inference on the 1,458-report held-out evaluation set before valid-span filtering.

The Qwen baselines were fine-tuned on the same 90/10 snapshot with the configuration in Table 9. Both used completion-only supervision, masking prompt tokens and preserving the target completion when inputs exceeded the model-specific length limit.

Table 9: LoRA SFT configuration for the Qwen3 baselines in the conditional extraction comparison. Effective batch size is per-device batch size multiplied by gradient accumulation.

Setting	Qwen3-0.6B	Qwen3-1.7B
LoRA rank / alpha / dropout	16 / 32 / 0.05	16 / 32 / 0.05
Target modules	Attention Q/K/V/O and feed-forward gate/up/down projections	
Bias / task type	none / causal LM	none / causal LM
Base precision / quantization	bf16 / no 4-bit	bf16 / no 4-bit
Maximum sequence length	4,096	2,048
Epochs	3	3
Per-device batch / accumulation / effective batch	1 / 16 / 16	1 / 16 / 16
Optimizer / learning rate	AdamW / 2×10^{-4}	AdamW / 2×10^{-4}
Schedule / warm-up	cosine / 3%	cosine / 3%
Weight decay / max gradient norm	0 / 1.0	0 / 1.0
Gradient checkpointing	enabled	enabled
Loss / seed	completion only / 42	completion only / 42

Qwen3-32B gold-key few-shot baseline. The Qwen3-32B constrained few-shot baseline obtains Exact, BTM-3, and Overlap F1 scores of 0.65612, 0.66274, and 0.71156 on the common evaluation subset of 1,242 reports under gold-key conditioning, with six parse failures.

A.4. Robustness and transfer analyses

DocILE inventory expansion. On the official DocILE split (5,179 training and 500 validation documents), training-ranked Top-5 and Top-20 inventories covered 45.40% and 88.71% of the 4,101 validation fields, recovering 1,540 and 2,919 exact fields, respectively. Conditional Exact/Overlap were 0.8271/0.8623 at Top-5 and 0.8024/0.8463 at Top-20.

Synthetic OCR-noise stress test. We applied synthetic character corruption to the 1,242-report common subset (substitution/deletion/insertion probabilities 0.60/0.25/0.15) and evaluated the BERT–BiLSTM–CRF conditional extractor. Table 10 is a controlled stress test, not an estimate of production OCR error rates.

Target CER	Measured CER	Exact F1	BTM-3 F1	Overlap F1
0%	0.000%	0.9060	0.9062	0.9711
2.5%	2.468%	0.6321	0.6325	0.7098
5%	4.982%	0.4813	0.4819	0.5684
10%	10.002%	0.3027	0.3028	0.4048
15%	14.998%	0.2063	0.2063	0.3037
20%	20.011%	0.1398	0.1400	0.2400

Table 10: Performance under synthetic character corruption.

Iterative versus one-shot clustering consistency. On the 536 surface keys shared by iterative and one-shot canonicalization, homogeneity is 0.9326, completeness is 0.9335, ARI is 0.3850, and directional purities are 0.8078 and 0.7873 (V-measure 0.9331 is reported in the main text). These measurements establish clustering consistency only.

A.5. Independent downstream utility study

Table 11 reports task-specific estimates from the independent utility study using 10,000 case-level paired bootstrap resamples (seed 42). TEXT is the text-only baseline; TEXT+STRUCT augments it with the structured representation.

Task	n	TEXT	STRUCT	TEXT+STRUCT	Δ vs. TEXT	95% paired bootstrap CI
Stage	578	0.7111	0.2976	0.7128	+0.17 pp	[-2.25, +2.60] pp
Histologic grade	672	0.8378	0.6057	0.8705	+3.27 pp	[+0.60, +5.95] pp
Treatment response	825	0.3042	0.1479	0.3394	+3.52 pp	[+1.45, +5.58] pp
Tumor recurrence	1,481	0.5078	0.4031	0.5219	+1.42 pp	[-0.07, +2.84] pp
5-year survival	578	0.1211	0.0121	0.0657	-5.54 pp	[-7.79, -3.46] pp
Primary site	1,581	0.9690	0.2460	0.9677	-0.13 pp	[-0.63, +0.38] pp

Table 11: Accuracy differences in the independent TCGA structured-representation utility study. TEXT, STRUCT, and TEXT+STRUCT are the three paired input arms; the last two columns report TEXT+STRUCT minus TEXT.